Parametric Study of Operation and Performance of a PEM Fuel Cell Using Numerical Method

Seddiq, Mehdi; Khaleghi, Hassan*[+]

Department of Mechanical Engineering, Faculty of Engineering, Tarbiat Modares University, Tehran, I.R. IRAN

Mirzaei, Masaud

Faculty of Aerospace Engineering, K.N. Toosi University of Technology, Tehran, I.R. IRAN

ABSTRACT: *Output characteristics of fuel cells are affected by a large number of parameters such as geometry, dimensions, construction materials and conditions of supplying fluids. In this paper a mathematical model followed by a two-dimensional numerical approach has been presented to study the fuel cell parametrically. Effect of oxygen concentration at gas diffusion layer entrance, temperature and pressure of the fluid in channels and thickness of membrane for various current densities were studied. The results show that increasing pressure and input oxygen concentration as well as decreasing membrane thickness improve power density and raise limiting current density.*

KEY WORDS: *Proton exchange membrane fuel cell, Parametric study, Numerical, Heat transfer, Mass transfer.*

INTRODUCTION

Proton exchange membrane fuel cell (PEMFC) has received most attentions today, due to its importance as an alternative for future vehicles power supply [1].

The principle of how a PEMFC works is very simple. As Fig. 1 shows, the primary materials, normally in gas phase, flow through separate channels. Channels are in adjacent with a gas diffusion layer (GDL) which lets the fluid to diffuse inside the cell. At the other side of the GDLs, a polymer membrane is sandwiched. The membrane is a hydrophilic porous media that adsorbs water like a sponge. The adsorbed water is converted to liquid phase, because its partial pressure exceeds saturation pressure. The hydrated membrane performs as a dam against reactant gases and prevents from direct contact between them. The two sides of the membrane are covered by a very thin layer of catalyst to facilitate reactions. Hydrogen is dissociated to proton and electron as it hits to anode catalyst layer:

$$H_2 \rightarrow 2H^+ + 2e^-$$

Hydrated membrane is a good conductance for proton and the proton migrates to cathode side where the oxygen is present. Oxygen reacts with proton on cathode catalyst:

$$2H^+ + 1/2O_2 + 2e^- \rightarrow H_2O$$

* *To whom correspondence should be addressed.*
+ *E-mail: khaleghi@modares.ac.ir*
1021-9986/08/2/1 12/$/3.20

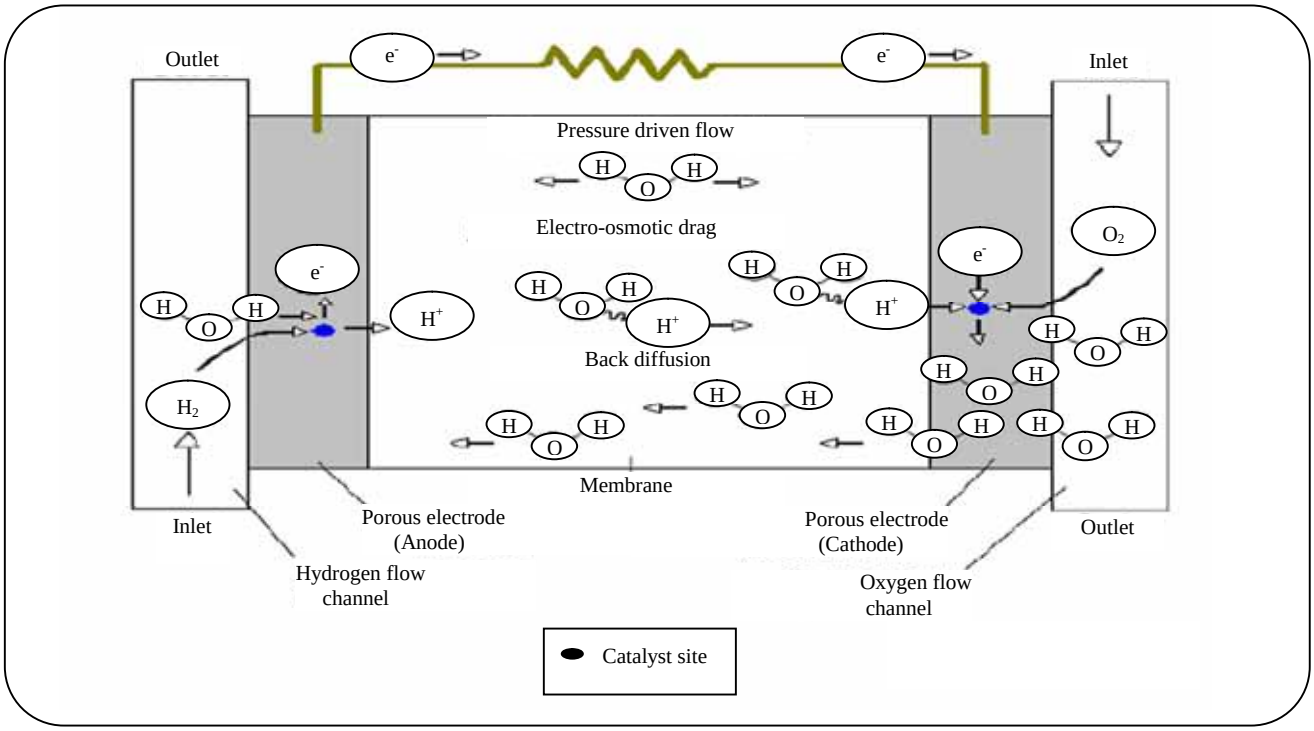

Fig. 1: Working principle of a PEM fuel cell ([2]).

The electrons of above reaction are supplied from anode (as a product of hydrogen dissociation) and are conducted through an electrical circuit. This current is the output DC power. A single fuel cell generates at most 1 volt electrical potential. In order to have enough potential, a lot of cells are connected in series.

Many efforts have been carried out for study and optimization of PEMFC. Experimental methods represent general insight to what occurs in fuel cells. These methods despite of their reliable results are expensive and involve numerous measurement limitations.

Detailed information of processes within the fuel cell over a wide variety of operating conditions may be obtained using numerical methods. During last 15 years, several numerical works have been accomplished ranging from simple one-dimensional to three-dimensional models. One-dimensional isothermal model of *Bernardi* and *Verbruge* [3] which contained only cathode was a base-frame for the next investigations. *Chu et al.* [4] derived a one-dimensional analytical-numerical model considering GDL with non-uniform porosity to study the effect of porosity on performance. *Singh et al.* [5] presented a two-dimensional model considering cross-sectional area normal to membrane as the solution domain. They used *Darcy* model instead of *Navier-Stocks* equations and emphasized on a better modelling of mass transfer. *Kermani et al.* [6] investigated importance of energy equation for prediction of liquid water formation in their two-dimensional work. In recent years three-dimensional models have been developed [7-9] to investigate various aspects of processes occurring in cell.

Here a two-dimensional non-isothermal model has been developed for simulation of fuel cell. Based on this model, a comprehensive study has been carried out to investigate effect of flow temperature, flow pressure, oxygen inlet concentration and membrane thickness on performance and operation of a fuel cell. This set of simulated parameters has not been considered in references. The gas cross-over through the membrane and the resulting direct reaction (whose importance has been evaluated in [10]) has been included in this model which has not been considered in the past researches.

MODEL DESCRIPTION

Fig. 2 depicts a general view of the present model. Five regions are included in solution domain: gas diffusion layers (anode and cathode), catalyst layers (anode and cathode) and membrane. Gas channels and bipolar plates are considered as boundaries.

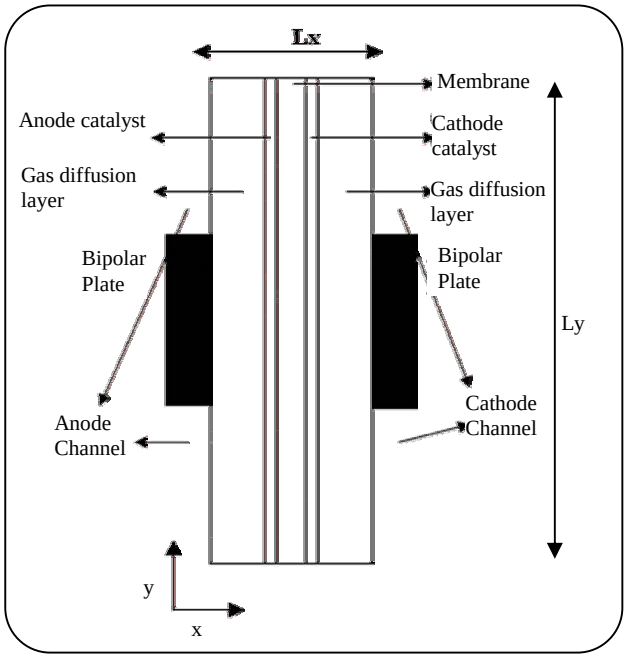

Fig. 2: Solution domain. Dimensions are exaggerated for better display.

The modelling assumptions in this study are as follows:

-The cell works under steady state conditions.

-The fluid in GDL is ideal gas. Volume of liquid water in this region is negligible and liquid phase has no effect on gas flow.

- The flow all over the cell is laminar.

- Product water is in form of liquid.

- GDL has infinite resistance against proton flow. So, all protons generated at anode catalyst migrate to cathode catalyst and react with oxygen.

- Porous media is in thermal equilibrium with the fluid.

- All crossed-over reactant gases are consumed in direct reaction, i.e. neither hydrogen exists in cathode GDL nor oxygen in anode GDL.

Governing Equations

The governing equations include Navier-Stocks and species transport equations that can be expressed as:

Continuity [10]

$$\frac{\partial(\varepsilon\rho)}{\partial t}+\nabla\cdot\left[\varepsilon\left(\rho\vec{u}+\dot{G}^{D}\right)\right]=Su^{mass} \qquad (1)$$

Where $\dot{G}^{D}$ is defined as diffusive mass flux [10]:

$$\dot{G}^{D}=\sum_{k}-D_{k}\nabla X_{k}\rho_{k} \qquad (2)$$

Su encompasses mass source/sink terms due to main reactions and electro-osmotic drag as is introduced for source terms of species transport equation [7,10]:

$$(Su)^{mass}=\sum_{k}\left[\left(Su_{k}^{R}+Su_{k}^{eod}\right)\rho_{k}\right]^{concentration} \qquad (3)$$

Momentum

$$\frac{\partial(\varepsilon\rho\vec{u})}{\partial t}+\nabla.(\varepsilon\rho\vec{u}\vec{u})=-\varepsilon\nabla P+\nabla.(\varepsilon\mu_{eff}\nabla\vec{u})-\frac{\varepsilon^{2}\mu}{K_{hy}}.\vec{u} \qquad (4)$$

The velocity used in the momentum equation is only due to convective mass transfer and diffusive velocity which originates from chaotic motions of molecules is not included.

Energy conservation

$$\frac{\partial(\rho C_{p}T)}{\partial t}+\nabla\cdot(\varepsilon\rho C_{p}\vec{u}T)=\nabla\cdot(k_{eff}\nabla T)+Su^{energy} \qquad (5)$$

Energy equation is applied for both porous media and fluid. So, treatment of interactions between these two phases is not needed, but the properties must be calculated as the average value of solid media and fluid. Source term consists of ohmic losses of proton current, activation over-potential and direct reaction [10]:

$$Su^{energy}=\begin{cases}\dfrac{i^{2}}{\sigma}+\left(V^{act}j+\dot{G}^{Cr}\cdot h_{react}\right)_{a}\\ \dfrac{i^{2}}{\sigma}\\ \dfrac{i^{2}}{\sigma}+\left(V^{act}j+\dot{G}^{Cr}\cdot h_{react}\right)_{c}\end{cases} \qquad (6)$$

i is current density magnitude.

Species transport

$$\frac{\partial(\varepsilon X_{k})}{\partial t}+\nabla\cdot(\varepsilon\vec{u}X_{k})=\nabla\cdot(D_{k}\nabla X_{k})+Su_{k}^{concentration} \qquad (7)$$

Subscript k denotes one of species (hydrogen, oxygen, water and probably nitrogen). Generally the source term includes consumption/production of species in main reaction and direct reaction and also specie transport under electro-osmotic drag. Nature of source term concerns to corresponding specie as follows:

Main reaction [7]

$$Su_{H_2}^{R}=\begin{cases}-\dfrac{j}{2FC_{tot}} & \text{anode catalyst}\\ 0 & \text{other locations}\end{cases} \quad (8)$$

$$Su_{O_2}^{R}=\begin{cases}-\dfrac{j}{4FC_{tot}} & \text{cathode catalyst}\\ 0 & \text{other locations}\end{cases}$$

$$Su_{Water}^{R}=\begin{cases}-\dfrac{j}{2FC_{tot}} & \text{cathode catalyst}\\ 0 & \text{other locations}\end{cases}$$

Direct reaction [10]

$$Su_{H_2}^{DR}=\begin{cases}\dfrac{\partial \dot{G}_{H_2}^{Cr}/\partial x}{C_{tot}} & \text{cathode catalyst}\\ 0 & \text{other locations}\end{cases} \quad (9)$$

$$Su_{O_2}^{DR}=\begin{cases}-\dfrac{\partial \dot{G}_{O_2}^{Cr}/\partial x}{C_{tot}} & \text{anode catalyst}\\ 0 & \text{other locations}\end{cases}$$

$$Su_{Water}^{DR}=\begin{cases}2\dfrac{\partial \dot{G}_{O_2}^{Cr}/\partial x}{C_{tot}} & \text{anode catalyst}\\ -\dfrac{\partial \dot{G}_{H_2}^{Cr}/\partial x}{C_{tot}} & \text{cathode catalyst}\\ 0 & \text{other locations}\end{cases}$$

C_{tot} denotes total volumetric mole of existing fluid. $\dot{G}_{O_2}^{Cr}$ is oxygen flow rates crossing over through membrane and contains both diffusion and convection. So the term $-\partial \dot{G}_{O_2}^{Cr}/\partial x$ denotes oxygen consumption rate. Similarly $\dot{G}_{H_2}^{Cr}$ is hydrogen flow rate from anode site to cathode catalyst. Note that the term $\partial \dot{G}_{H_2}^{Cr}/\partial x$ is inherently negative.

Electro-osmotic drag

$$Su^{eod}=-\frac{\nabla \vec{i}\cdot n^{eod}}{FC_{tot}} \quad (10)$$

$\vec{i}$ is current density vector indicating both magnitude and direction of protons migration.

Dissolving

When a gas is in contact with liquid, some molecules penetrate in the liquid and are dissolved. Simultaneously some dissolved molecules pass through the liquid surface and escape to gas phase. The value of dissolved gas in liquid surface falls at equilibrium point in which the entering rate is equal with exiting rate:

$$C_k^s=\frac{1}{H}X_k^g P \quad (11)$$

where H is *Henry's* law constant.

Normally, the species transport equation is solved for 3 species hydrogen, oxygen and water. Nitrogen concentration is then calculated easily:

$$X_{N_2}=1-X_{H_2}-H_{O_2}-X_{Water} \quad (12)$$

Phase potential (proton transport)

$$\nabla(\sigma\nabla\Phi)=Su^{\Phi} \quad (13)$$

Where:

$$Su^{\Phi}=\begin{cases}+j & \text{anode catalyst}\\ -j & \text{cathode catalyst}\\ 0 & \text{other locations}\end{cases} \quad (14)$$

Fluid Properties and electrochemical quantities

Density

$$\rho=C_{tot}\sum_k X_k M_k \quad (15)$$

Viscosity

$$\mu=\frac{\rho_k\mu_k}{\rho}=\frac{\sum_k X_k M_k \mu_k}{\sum_k X_k M_k} \quad (16)$$

effective viscosity for porous media is [13]:

$$\mu_{eff}=\left[\frac{1.5(1-\varepsilon)}{\varepsilon}\right]^2\mu \quad (17)$$

Effective thermal conductivity [13]

$$K_{eff}=-2K_S+\frac{1}{\dfrac{\varepsilon}{2K_S+K_f}+\dfrac{1-\varepsilon}{3K_S}} \quad (18)$$

$$K_f = \sum_k X_k K_k \quad (19)$$

Heat capacity

$$\rho Cp = \varepsilon(\rho Cp)_f + (1-\varepsilon)(\rho Cp)_S \quad (20)$$

$$(\rho Cp)_f = \sum_k \rho_k Cp_k = C_{tot} \sum_k X_k M_k Cp_k \quad (21)$$

Mass diffusion coefficients

For gas phase we have [8]:

$$D_k^g = D_k^{ref} \left(\frac{T}{T^{ref}} \right)^{1.5} \left(\frac{P^{ref}}{P} \right) \quad (22)$$

In dissolved form diffusion coefficient obeys another relation [11]:

$$D_k^S = c \frac{T}{\mu} \quad (23)$$

μ denotes solvent (water) viscosity. c for each solute gas is a constant.

For liquid water [10]:

$$D_{water}^l = D_i e^{2416(\frac{1}{303} - \frac{1}{T})} \quad (24)$$

$$D_i = \begin{cases} 10^{-10} & \lambda < 2 \\ 10^{-10}(-3+2\lambda) & 2 < \lambda \le 2 \\ 10^{-10}(6.5-1.167\lambda) & 3 < \lambda \le 4.5 \\ 1.25\times10^{-10} & 4.5 \le \lambda \end{cases} \quad (25)$$

λ is water content in membrane.

Proton conductivity [9,10,13]

$$\sigma = (0.5139\lambda - 0.326) e^{1268(\frac{1}{303} - \frac{1}{T})} \quad (26)$$

Water content in membrane [9,10,13]

$$\lambda = \begin{cases} 0.043 + 17.18a_w - 39.85a_w^2 + 36.0a_w^3 & 0 < a \le 1 \\ 14.0 + 1.4(a_w - 1) & 1 \le a \le 3 \\ 16.9 & 3 < a \end{cases} \quad (27)$$

Activity of water

$$a_w = \frac{X_{water} P}{P_{sat}} \quad (28)$$

Water concentration in membrane

$$C_{water} = \lambda \frac{\rho_m}{M_m} \quad (29)$$

Total mole of matter per volume

In gas phase: $C_{tot}=P/RT$ (30 A)

In liquid phase: $C_{tot}=C_{Water}/X_{Water}$ (30 B)

Electro-osmotic drag coefficient [9,10]

$$n^{eod} == 0.0029\lambda^2 + 0.05\lambda - 3.4\times10^{-19} \quad (31)$$

Current density in membrane

$$\vec{i} = -\sigma \nabla \Phi \quad (32)$$

Transfer current density

$$j = \nabla \vec{i} \quad (33)$$

Activation over-potential at catalysts

$$V_a^{act} = \frac{RT}{F} \ln\left(\frac{i}{i_a^{ref} X_{H_2}}\right) \quad (34\ A)$$

$$V_c^{act} = \frac{2RT}{F} \ln\left(\frac{i}{i_c^{ref} X_{O_2}}\right) \quad (34\ B)$$

Cell voltage

$$V^{cell} = E^0 - \left(\int_a^c \frac{x}{\sigma} dx + V_a^{act} + V_c^{act} \right) \quad (35)$$

Power density

$$\dot{w} = iV^{cell} \quad (36)$$

Numerical procedure

A finite volume code was developed to solve the governing equations.Two grid networks have been used, one for scalar variables and the other (staggered grid) for vector variables (velocity and current density) to enhance the accuracy in calculation of gradients.

Power law scheme was applied for approximation of diffusion/convection fluxes on control volume faces. To decouple equations, SIMPLE [12] algorithm was used and convergence was obtained with iteration. The numerical method converged after 2400-7000 iterations, depending on the case. Very wise selection of relaxation factors is necessary to prevent divergence.

Table 1: Physical parameters and properties. Values for gases dissolution and diffusivity in water have been adopted or calculated from [11], porous media properties are from [13].

parameter	Unit	Value
ε in GDL	-	0.4
ε in membrane and catalyst	-	0.25
K_{hy} in GDL	m^2	1.76×10^{-11}
K_{hy} in membrane	m^2	1.8×10^{-18}
ρ_m	kg m^{-3}	1840
M_m	kg $mole^{-1}$	1.1
i^{ref} at anode	A m^{-2}	100
i^{ref} at cathode	A m^{-2}	1000
T^{ref}	K	353
P^{ref}	kPa	101.325
h_{reat}	J kg^{-1}	-285830
R	J kg^{-1} K^{-1}	8.314
F	C $mole^{-1}$	96487
$D^{ref}_{H_2}$	m^2 s^{-1}	1.1×10^{-4}
$D^{ref}_{O_2}$	m^2 s^{-1}	3.2×10^{-5}
D^{ref}_{Water}	m^2 s^{-1}	7.35×10^{-5}
$D^{S}_{H_2}$ at 353 K	m^2 s^{-1}	2.59×10^{-10}
$D^{S}_{O_2}$ at 353 K	m^2 s^{-1}	1.22×10^{-8}
$H_{H_2} = (K_1/K_2)_{H_2}^{\text{at 353 K}}$	Pa m^3 $mole^{-1}$	3.2886×10^{4}
$H_{O_2} = (K_1/K_2)_{O_2}^{\text{at 353 K}}$	Pa m^3 $mole^{-1}$	2.0265×10^{4}

Table 2: Specifications and operating conditions for the base case.

parameter	Unit	Value
$R_{O\text{-}N}$ at cathode channel entrance	$mole.mole^{-1}$	0.266
Fluid temperature at anode channel	K	353
Fluid temperature at cathode channel	K	353
Pressure at anode channel	atm	3
Pressure at cathode channel	atm	3
RH at anode channel entrance	%	95
RH at cathode channel entrance	%	50
Gas diffusion layers thickness	μm	200
Catalysts thickness	μm	20
Membrane thickness	μm	108
Cell width (Ly)	μm	2000
Bipolar plates width	μm	800

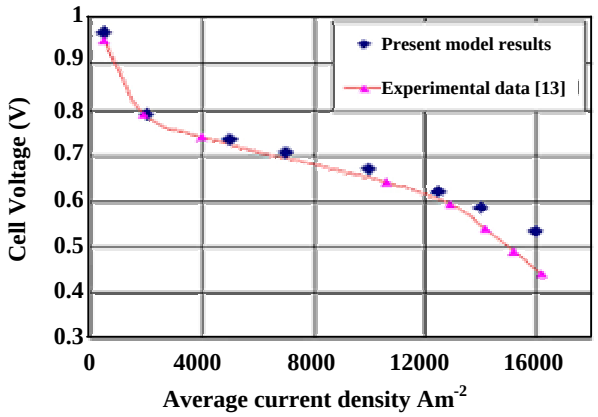

Fig. 3: Polarization Curve, validation of the model with experimental data.

RESULTS AND DISCUSSION

Physical parameters and properties are listed in table 1. A set of dimensions and operating conditions was selected as a base for comparison of different cases and also validation of the model. Several simulations were carried out to obtain grid independent results. The grid and corresponding operating conditions for the base case have been presented in table 2.

Fig. 3 compares predicted polarization curve with experimental data reported by *Wang et al.* [13]. A satisfactory accuracy is observed up to current density of 1250 Am^{-2}. At high current densities, the presented model over-predicts cell voltage. This is due to formation of liquid water in cathode GDL. At high current densities we have more water production and consequently liquid water may be formed within the GDL. The liquid water clogs porous media and disturbs oxygen flow from channel to catalyst. Consequently cathode activation over-potential is increased and cell potential is decreased. A single-phase model is not able to simulate this process. However the presented model can be used for a wide range of current densities up to the two-phase threshold.

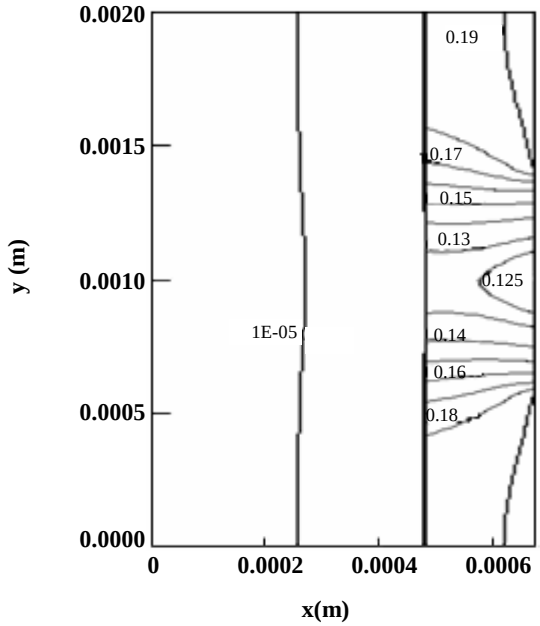

Fig. 4: Oxygen mole fraction (mole O_2 per total mole gas) contours.

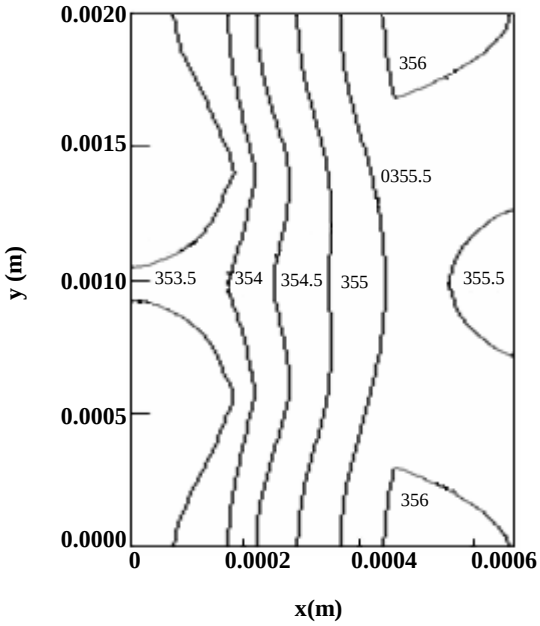

Fig. 5: Temperature (K) contours.

A general view upon the cell

Fig. 4 displays oxygen concentration in the cell. This figure shows that oxygen diffuses from cathode channel to catalyst.

A discontinuity is observed at GDL-catalyst interface, because oxygen should be dissolved in water to enter membrane region and molar concentration of free oxygen is about 9 times greater than that in dissolved form. Oxygen concentration in GDL takes its minimum value adjacent to y=Ly/2 axis, because this location is relatively far from channels.

Temperature field is presented in Fig. 5. In cathode side we have 2-2.5 K increase in temperature while in anode the temperature rise is only 0.5-1 K. The main reason of this difference is higher value of activation energy in cathode catalyst.

A parametric analysis

Here we have four important input parameters including: oxygen to nitrogen volumetric ratio, temperature and pressure of fluid in channels and membrane thickness. The effects of these parameters on minimum concentration of oxygen and maximum relative humidity in cathode GDL (limiting parameters), cell power density (performance parameter) and maximum temperature within the cell (explanatory parameter) are investigated.

Effect of oxygen concentration in cathode channel

Study of this parameter helps us to understand effect of oxygen concentration variation along the channels which is normally simulated in a 3D model. Here the volumetric ratio of oxygen to nitrogen at cathode channel entrance has been selected as the variable representing oxygen concentration. $R_{O\text{-}N}=\infty$ and $R_{O\text{-}N} = 0.266$ correspond to pure oxygen and standard air mixture, respectively. In all cases according to table 2, a 50 % relative humidity has been assumed for gases mixture at cathode channel entrance.

Minimum concentration of oxygen in mole per volume is a bottle neck for maximum possible current density. As current density rises, oxygen concentration in cathode catalyst is decreased. Theoretically, there is a certain current density, namely the limiting current density, which makes oxygen concentration zero and no more current could be achieved. It is evident that decreasing the oxygen concentration in channels leads its minimum concentration to diminish within the cell (see Fig. 6) and activation over-potential is increased. Consequently as it is seen in Fig. 7, we have smaller power density. Fig. 7 also shows that power density curves are ascending but the slope rate is descending due to voltage reduction.

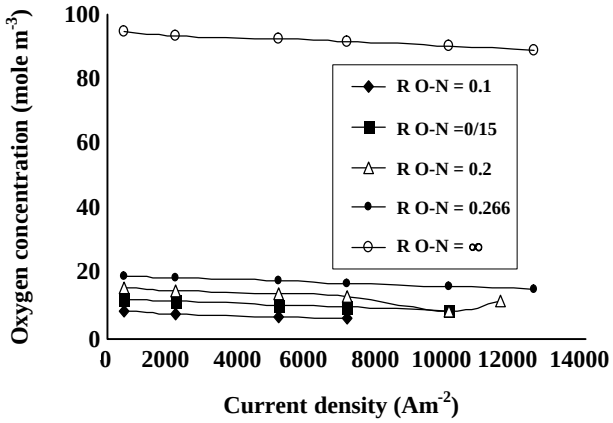

Fig. 6: Minimum Concentrations of oxygen within cathode GDL versus current density for various values of $R_{O\text{-}N}$.

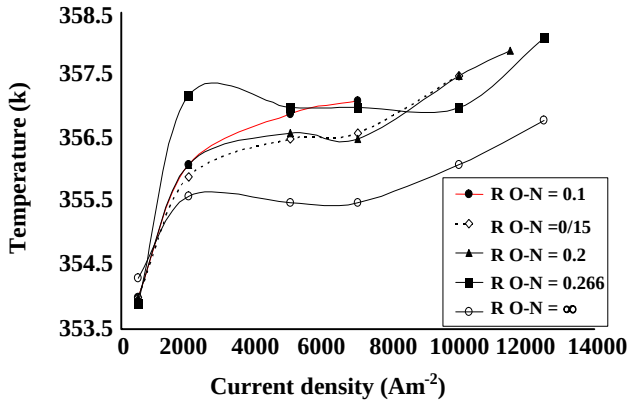

Fig. 8: Maximum temperatures within the cell versus current density for various values of $R_{O\text{-}N}$.

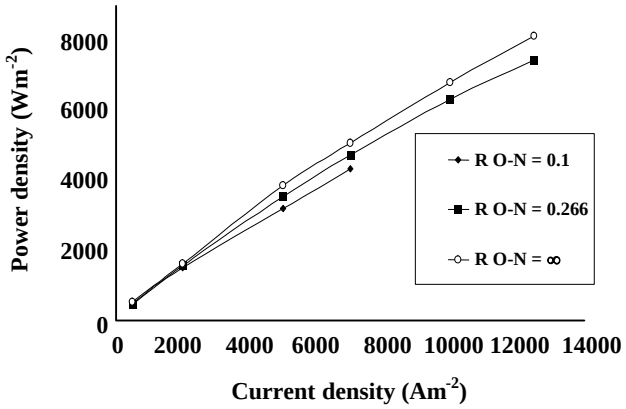

Fig. 7: Power density versus current density for various values of $R_{O\text{-}N}$.

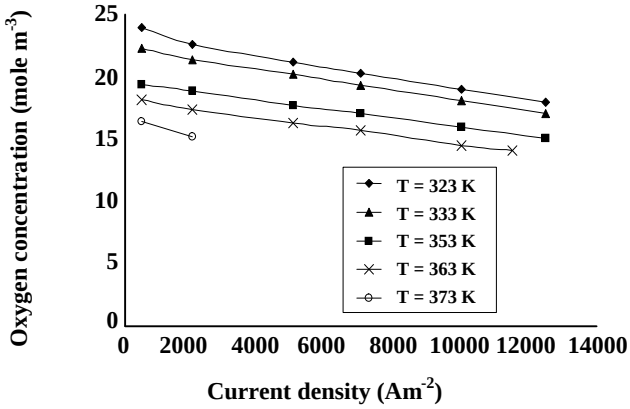

Fig. 9: Minimum concentrations of oxygen within cathode GDL versus current density for various temperatures of channels fluid.

The energy loss due to activation over-potential is released in form of heat and causes the cell to be warmer. This is why in case of pure oxygen we have minimum increase in temperature, according to Fig. 8. Consequently, relative humidity will be slightly more than that of the case in which the cell is fed with dilute oxygen.

Separate simulations show that as the concentration of oxygen is increased, the energy losses due to direct reaction at anode is increased. This may be deduced as a drawback of using pure oxygen instead of air.

Effect of fluid temperature in channels

Total mole per volume is inversely proportional to temperature. So with a higher temperature we have smaller oxygen concentration (Fig. 9) and greater activation over-potential, but the open-circuit voltage (E^0) is also increased so that we have finally greater cell voltage. Fig. 10 shows that power density is increased with temperature. Power density curves are divergent because rise in open-circuit voltage is more obvious at higher current densities.

Channel temperature affects cell temperature directly. Here the temperature increment, i.e. maximum temperature within the cell minus channel temperature is of interest. Variation of this quantity versus current density has been displayed in Fig. 11 for various channel temperatures. The outstanding observation in this figure is that with a lower channel temperature, we have more increase in cell temperature. For explanation, it must be noted that temperature affects both thermal properties and

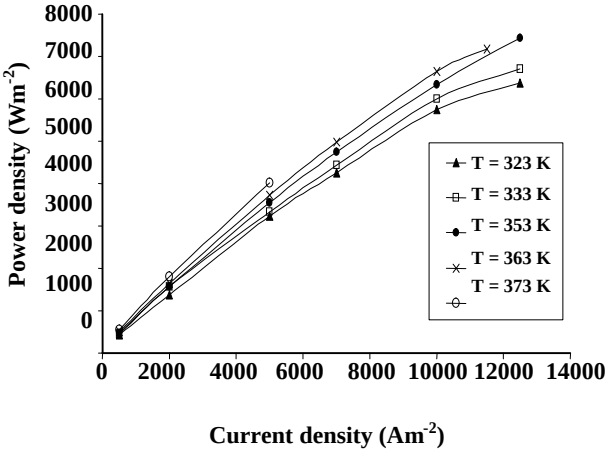

Fig. 10: Power density versus current density for various temperatures of channels fluid.

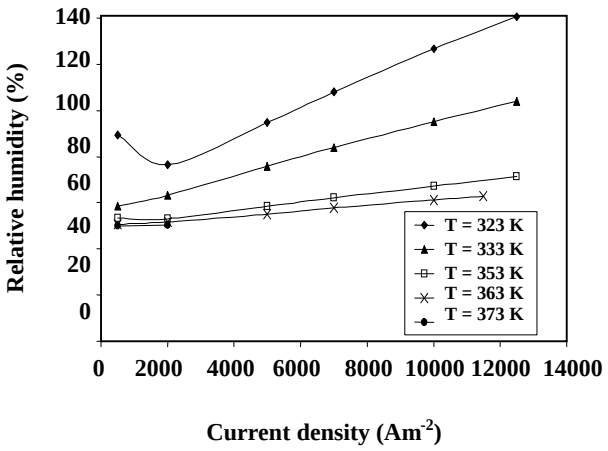

Fig. 12: Maximum relative humidity within cathode GDL versus current density for various temperatures of channels fluid.

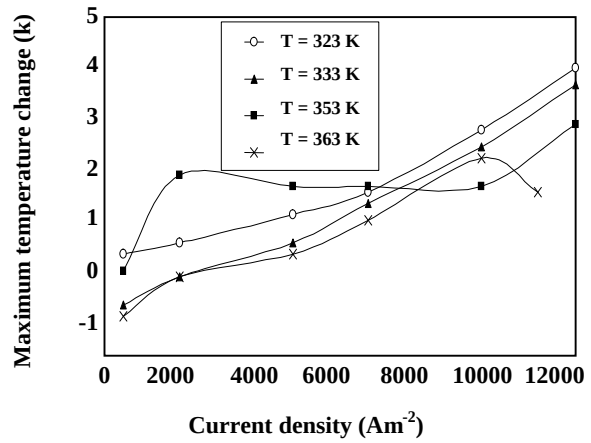

Fig. 11: Maximum temperature changes within the cell versus current density for various temperatures of channels fluid.

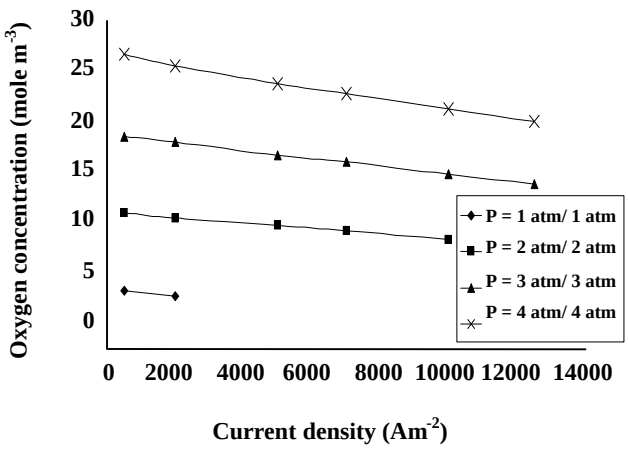

Fig. 13: Minimum concentrations of oxygen within cathode GDL versus current density for various pressures of anode/cathode channels.

source terms. As temperature is increased, fluids thermal conductivity and slightly heat capacity are increased. This causes temperature gradients to be moderated and attenuates temperature rise. The source terms are also dependent on temperature. Both proton conductivity and activation over-potential are increased when temperature is increased (equations (26) and (34)). For instance, if temperature varies from 323 K to 363 K, proton conductivity is increased 35 % which decreases ohmic losses by 35 % generation.

Effect of temperature on relative humidity is very important. Fig. 12 illustrates maximum relative humidity curves. for channel temperature of 323 K the saturation threshold falls at current density of 5800 Am^{-2}, while for temperature of 333 K the saturation threshold is postponed to 11200 Am^{-2} and in higher simulated temperatures, saturation does not occur at current densities less than 12500 Am^{-2}.

Effect of pressure

Fig. 13 displays minimum oxygen concentrations for various pressures. As was expected, since total mole per volume is proportional to pressure, oxygen concen-tration and hence power density are increased with pressure (Fig. 14).

No obvious change can be seen in maximum tempe-rature with pressure variations. It was found that maximum relative humidity is slightly increased with pressure.

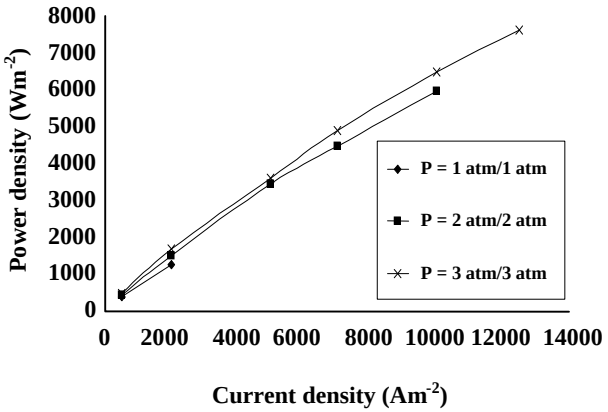

Fig. 14: Power density versus current density for various pressures of anode/cathode channels.

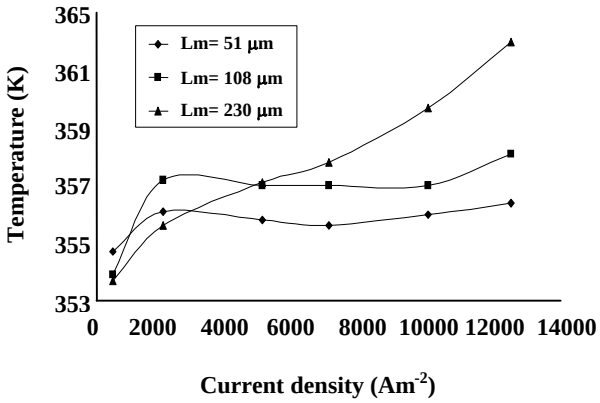

Fig. 16: Maximum temperatures within the cell versus current density for various thicknesses of membrane.

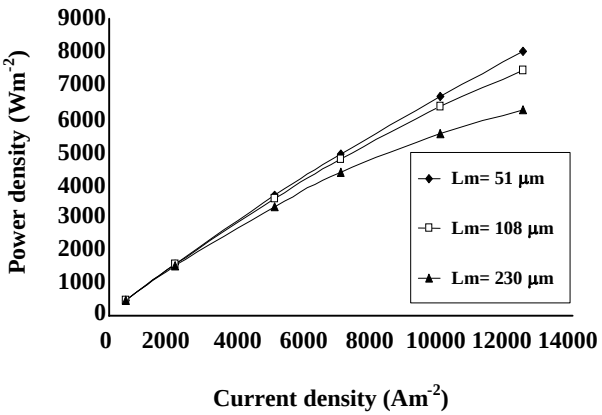

Fig. 15: Power density versus current density for various thicknesses of membrane.

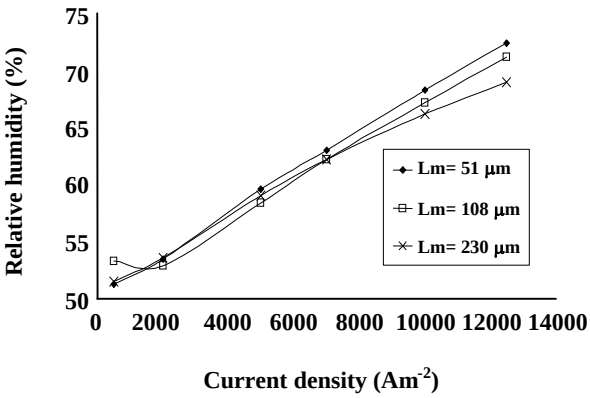

Fig. 17: Maximum relative humidities within cathode GDL versus current density for various thicknesses of membrane.

Effect of membrane thickness

Membrane thickness has a negligible effect on oxygen concentration, but since it directly affects ohmic losses, cell power e specially at high current densities, is decreased when thicker membrane is used (Fig. 15).

Fig. 16 shows variations of maximum temperature for various membrane thicknesses. Thicker membrane will cause more heat generation, due to Ohmic losses and consequently higher temperature within the cell. This is why maximum relative humidity in cathode is decreased a little for a cell with thicker membrane (Fig. 17).

CONCLUSIONS

A PEM fuel cell was studied for a vast range of fluid conditions in channels (oxygen/nitrogen ratio, temperature and pressure) and different thicknesses for membrane.

Mole fraction of oxygen at cathode channel entrance affects minimum concentration of oxygen close to catalyst. A greater value for this parameter enhances output power and decreases heating of the fluid during cell operation especially at high-load conditions. Moreover the fuel cell can operate at greater current densities. Temperature of fluid in channels influences the fluid properties and electro-chemical processes within the cell. A warmer fluid contains smaller amounts of both reactant gas and water per volume. So, two influential factors in determination of maximum possible current density are changed: minimum oxygen concentration and maximum relative humidity. The former acts as a limitation, while the latter postpones saturation and enables the cell to work at higher current densities. Besides these advantages and drawbacks, cell voltage is increased as the fluids temperature is increased and also lower heat is released.

High pressure conditions affect minimum oxygen concentration and maximum relative humidity similar to low temperature conditions. But its effect on oxygen concentration is more obvious. So a greater pressure especially in cathode channels improves output power and enables fuel cell to have greater current densities.

Thickness of membrane mainly affects Ohmic losses and should be selected as small as possible considering construction/assembly limitations and also risk of reactant gases cross-over.

Nomenclatures

a_w	Water activity
C	Concentration (mole m^{-3})
Cp	Specific heat capacity (J kg^{-1} K^{-1})
D	Mass diffusion coefficient (m^2 s^{-1})
E^0	Open circuit cell voltage
F	Faraday constant (C $mole^{-1}$)
GDL	Gas diffusion layer
$\dot{G}$	Mass flux (kg m^{-2} s^{-1}) or (mole m^{-2} s^{-1})
H	*Henry's* law constant (Pa m^3 $mole^{-1}$)
h_{reac}	Liquid water enthalpy of formation (J $mole^{-1}$)
$\vec{i}$	Current density vector (A m^{-2})
j	Transfer current density (A m^{-3})
k	Thermal conductivity (W m^{-1} K^{-1})
K_{hy}	Hydraulic permeability of porous media (m^2)
Lx, Ly	Dimensions see Fig. 1 (m)
M	Molar weight (kg $mole^{-1}$)
M_m	Membrane molar weight (kg $mole^{-1}$)
n_{eod}	Electro-osmotic drag coefficient
P	Pressure (kPa)
P_{sat}	Saturation pressure (kPa)
R	Gas constant (J $mole^{-1}$ K^{-1})
RH	Relative humidity
R_{O-N}	Volumetric ratio of O_2 to N_2
Su	Non-homogeneous source term
Sp	Homogeneous source term
T	Temperature (K)
$\vec{u}$	Velocity vector (m s^{-1})
V^{cell}	Actual cell voltage (V)
V^{act}	Activation over-potential (V)
$\dot{w}$	Power density (W m^{-2})
X	Concentration (mole fraction)
x, y	Coordinates (m)
ε	Porosity
ϕ	Phase potential (V)
λ	Water content (mole water/mole SO_3^{2-})
μ	Viscosity (kg m^{-1} s^{-1})
ρ	Density (kg m^{-3})
ρ_m	Dry membrane density (kg m^{-3})
σ	Proton conductivity (Ω^{-1} m^{-1})

Superscripts

Cr	Cross-over
D	Diffusion
DR	Direct reaction
eod	Electro-osmotic drag
g	Gas
R	Main reaction
ref	Reference
S	Solute, dissolution

Subscripts

a	Anode
c	Cathode
eff	Effective
f	Fluid
k	Species (hydrogen, oxygen, water or nitrogen)
s	Solid media

Received : 11th November 2005 ; Accepted : 16th March 2008

REFERENCES

[1] Larminie, J. and Dicks, A., "Fuel Cell Explained", 2nd Ed., John Wiley & Sons, West Sussex, pp. 1-14, 53-59 (2003).

[2] Evans, J.P., Ellis, M.W., Von Spakovsky, M.R., Nelson, D.J., Experimental Evaluation of the Effect of Inlet Gas Humidification on Fuel Cell Performance, M.S. Thesis for Mechanical Engineering in Virginia Polytechnic and State University, (2003).

[3] Bernardi, D.N. and Verbrugge, M.W., Mathematical Model of a Gas Diffusion Electrode Bonded to a Polymer Electrolyte, *AIChE J.*, **37**, 1151 (1991).

[4] Chu, H.S., Yeh, C., Chen, F., Effects of Porosity Change of Gas Diffuser on Performance of Proton Exchange Membrane Fuel Cell, *J. of Power Sources*, **123**, 1 (2003).

[5] Singh, D., Lu, D.M., Djilali, N., A Two-Dimensional Analysis of Mass Transport in Proton Exchange Membrane Fuel Cells, *Int. J. of Engineering Science*, **37**, 431 (1999).

[6] Kermani, M.J., Stockie, J.M., Gerber, A.G., Condensation in the Cathode of a PEM Fuel Cell, 11th Annual Conference of CFD Society of Canada.

[7] Berning, T., Lu, D.M., Djilali, N., Three-Dimensional Computational Analysis of Transport Phenomena in a PEM Fuel Cell, *J. of Power Sources*, **106**, 284 (2002).

[8] Um, S. and Wang, C.Y., Three-Dimensional Analysis of Transport and Electrochemical Reactions in Polymer Electrolyte Fuel Cells, *J. Power Sources*, **125**, 40 (2004).

[9] Meng, H. and Wang, C.Y., Electron Transport in PEFCs, *J. of The Electrochemical Society*, **151(3)**, A358 (2004).

[10] Seddiq, M., Khaleghi, H. and Mirzaei, M., Numerical Analysis of Gas Cross-Over through the Membrane in a Proton Exchange Membrane Fuel Cell, *J. Power Sources*, **161(1)**, 371 (2006).

[11] Perry, R.H. and Chilton, C.H., "Chemical Engineers' Handbook", Fifth Ed., McGraw-Hill, Tokyo, pp. 3_96-3_98, 3_222-3_235 (1982).

[12] Patankar, S.V., "Numerical Heat Transfer and Fluid Flow, Hemisphere", New York, (1980).

[13] Wang, L., Husar, A., Zhou, T., Liu, H., A Parametric Study of PEM Fuel Cell Performances, *Int. J. Hydrogen Energy*, **28**, 1263 (2003).